Inhomogeneous spatial modelling of DPT pulses for marine images

Inger Fabris-Rotelli

University of Pretoria, South Africa

Alfred Stein

University of Pretoria, South Africa and University of Twente, Netherlands

Abstract

The Discrete Pulse Transform (DPT) is a nonlinear decomposition of a signal and extracts the structures in a signal at discrete scale levels. This study models the image structure extracted using the DPT as connected components. For this purpose, the Matérn cluster process is being used as it mimics the pulses of the DPT as clusters. In this paper it is applied to a marine image. Inhomogeneity of the pattern is dealt with by means of the fitted intensity. The model residuals exhibited the same pattern as the original image, and a refit resulted in residuals without pattern. The study concludes that the Matérn cluster model well fits the pulses obtained using the DPT and is well able to model the wave pulses of the ocean surface as clusters. This type of hierarchical cluster modeling presents interesting opportunities for simulations via conditioning.

Keywords: Discrete Pulse Transform, Matérn cluster process, Spatial modelling, inhomogeneity, LULU operators, big spatial data

1. Introduction

With modern sensors, images of an increasing size are being obtained. This applies to both images taken from satellites as well as for images taken by professional and handheld devices. A common use of images is automatic object recognition. LULU theory for images [1] has been developed in the past and has by now found a general acceptance. It has found a particular place in segmentation and object detection, whereas its potential to use it for noise removal has been reported in [2, 3, 4, 5]. Refinement of applications, however, is still very much at large. The LULU operators L_n and U_n, at discrete scale n, are smoothers operating in $\mathbb{Z}^d$ using maximum and mimimum operations iteratively. For the case $d = 2$ the smoothing of images specifically is attained. They are nonlinear smoothers and have many useful smoothing properties [1].

*Corresponding author

Email address: inger.fabris-rotelli@up.ac.za (Alfred Stein)

Various types of images contain longitudinal objects. One may think of images taken from the sea, where waves are clearly visible, or images taken in a forest, satellite images focusing on natural objects like roads and dykes [6] and incisions in several types of medical images. On all such images, it is important to separate the objects, be it waves, trees, geological faults or human texture elements from their background. In addition, their relative positioning is important, which we will model as the pattern of objects.

In this paper we focus specifically on marine images where the question is to identify waves as objects. A water surface is relatively complicated as the angle of view requires one to incorporate a change in scale with the texture as we move towards pulses on the horizon; waves can be smooth or rough at a varying degree, are foamy or not; also solar glint cause intense spikes in the water 'colour' which has to be accounted for. Existing models for water simulation make use of physical models to deal with glint [7, 8, 9, 10, 11, 12, 13] and to simulate water (generally for computer graphics) [14, 15, 16, 17, 18, 19, 20]. A model using a statistical texture model has not been attempted so far. Discussions on texture analysis of natural scenes can be found in [21], [22] and [23]. Here, water texture is described as partly stochastic and partly structural.

The LULU operators are able to well distinguish individual elements, but have to date not been investigated for their ability to quantify a pattern. In order to proceed, we turn to spatial statistics, in particular point pattern methods, where the aim is to model the occurrence of point objects as a function of their separation distance. These methods have been proven to be useful for quantifying patterns of e.g. trees, earthquakes, landslides and deforested patches in the Amazonian forest. Their emphasis has been on objects that can essentially be reduced to points. For object modelling, however, as far as we know the methods have not been explored. It is therefore a promising direction to combine the elements of spatial statistics to improve the application of the LULU image operators. We do so by focusing on the pulses obtained through the Discrete Pulse Transform (DPT) of an image. Each pulse is represented as an object in a spatial domain.

The DPT is a nonlinear multi-scale decomposition of an image obtained through recursive application of the operators L_n and U_n into connected constant valued groups of pixels over all possible discrete scales (equivalent to the number of pixels in a group) in the image [1]. The pulses obtained from the DPT provide useful constructs for background modelling of images. The image in Figure 1(a) from the Brodatz texture database[1] and images (b) - (d) in Figure 1 shows waves against a dark background. Objects are clearly horizontal, whereas there is a change in wave size from the front of the image towards the horizon. This change in size requires specific modeling, as there is no reason to assume that the distribution of relative wave sizes are different nearby as compared to that at a

[1] http://www.ux.uis.no/ tranden/brodatz.html

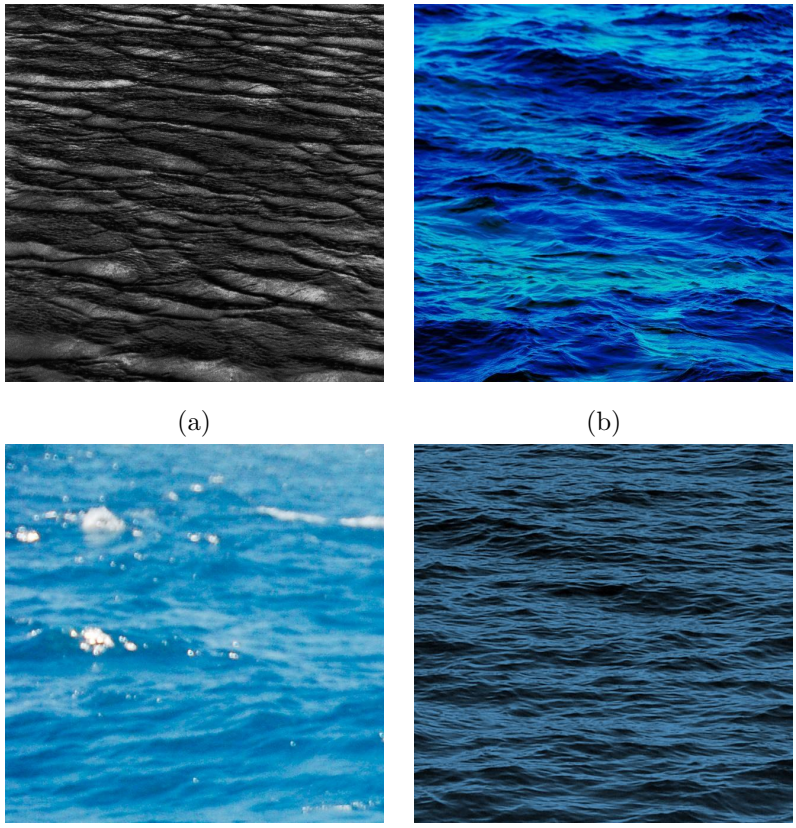

(a) (b)

(c) (d)

Figure 1: Examples of water images ((a) is from the Brodatz texture database, (b) - (d) are real images) all of size 640×640 pixels

further distance. In spatial modelling this implies an inhomogenenous pattern with a specific direction for the change in intensity, that is, from front to back. Furthermore, each pulse obtained from the DPT has a specific size as well as a shape, so that the variety of shapes provides information on the textures of the pattern of the pulses. The DPT pulses, grouped appropriately, provide information on separate waves which can be obtained through quantifying the pattern of the pulses. As far as we are aware, relations between the DPT and spatial statistics have not been investigated.

The aim of this paper is to present a point process modeling approach of the pulses at the scales which capture the pattern of the image. The study is applied on the images (greyscale versions) in Figure 1, and clustering characteristics of such marine images are discussed. This is a new approach to the pulses of the DPT and provides insight to their spatial nature inherent in images.

2. Point patterns resulting from the DPT

Let B be an arbitrary non-empty set. A family $\mathcal{C}$ of subsets of B is called a connected class or a connection on B [24] if

(i) $\emptyset \in \mathcal{C}$

(ii) $\{x\} \in \mathcal{C}$ for all $x \in B$

(iii) for any family $\{C_i\}_{i\in I} \subseteq \mathcal{C}$ we have $\bigcap_{i\in I} C_i \neq \emptyset \Longrightarrow \bigcup_{i\in I} C_i \in \mathcal{C}$.

If a set C belongs to a connection $\mathcal{C}$ then C is called connected.

The LULU operators were first developed for one dimensional signals on $\mathbb{Z}$, which is a fully ordered domain. The extension to $\mathbb{Z}^d, d \geq 2$ requires the concept of a connection to define the neighbours in higher dimensions (see [1] for more details). The Discrete Pulse Transform (DPT) is obtained via the sequential application of the LULU operators L_n and U_n, $n = 1, 2, .., N$ where N is the total number of pixels in the image. They are defined following [1], for $f \in \mathcal{A}(\mathbb{Z}^2)$, a vector lattice, and $n \in \mathbb{N}$, as

$$\begin{aligned} L_n(f)(x) &= \max_{V\in\mathcal{N}_n(x)} \min_{y\in V} f(y),\ x \in \mathbb{Z}^2\ , \\ U_n(f)(x) &= \min_{V\in\mathcal{N}_n(x)} \max_{y\in V} f(y),\ x \in \mathbb{Z}^2\ , \end{aligned}$$

where $\mathcal{N}_n(x) = \{V \in \mathcal{C} : x \in V, \mathrm{card}(V) = n + 1\}$ and $\mathcal{C}$ is a connection defined as above. L_n and U_n act as area openings and closings [25] respectively. The LULU operators act only on local maximum and local minimum sets. A connected subset V of $\mathbb{Z}^d$ is called a local maximum set of $f \in \mathcal{A}(\mathbb{Z}^d)$ if

$$\sup_{y\in \mathrm{adj}(V)} f(y) < \inf_{x\in V} f(x),$$

where $\mathrm{adj}(V)$ is the set of neighbouring pixels of V defined according to the connection $\mathcal{C}$. Similarly V is a local minimum set if

$$\inf_{y\in \mathrm{adj}(V)} f(y) > \sup_{x\in V} f(x).$$

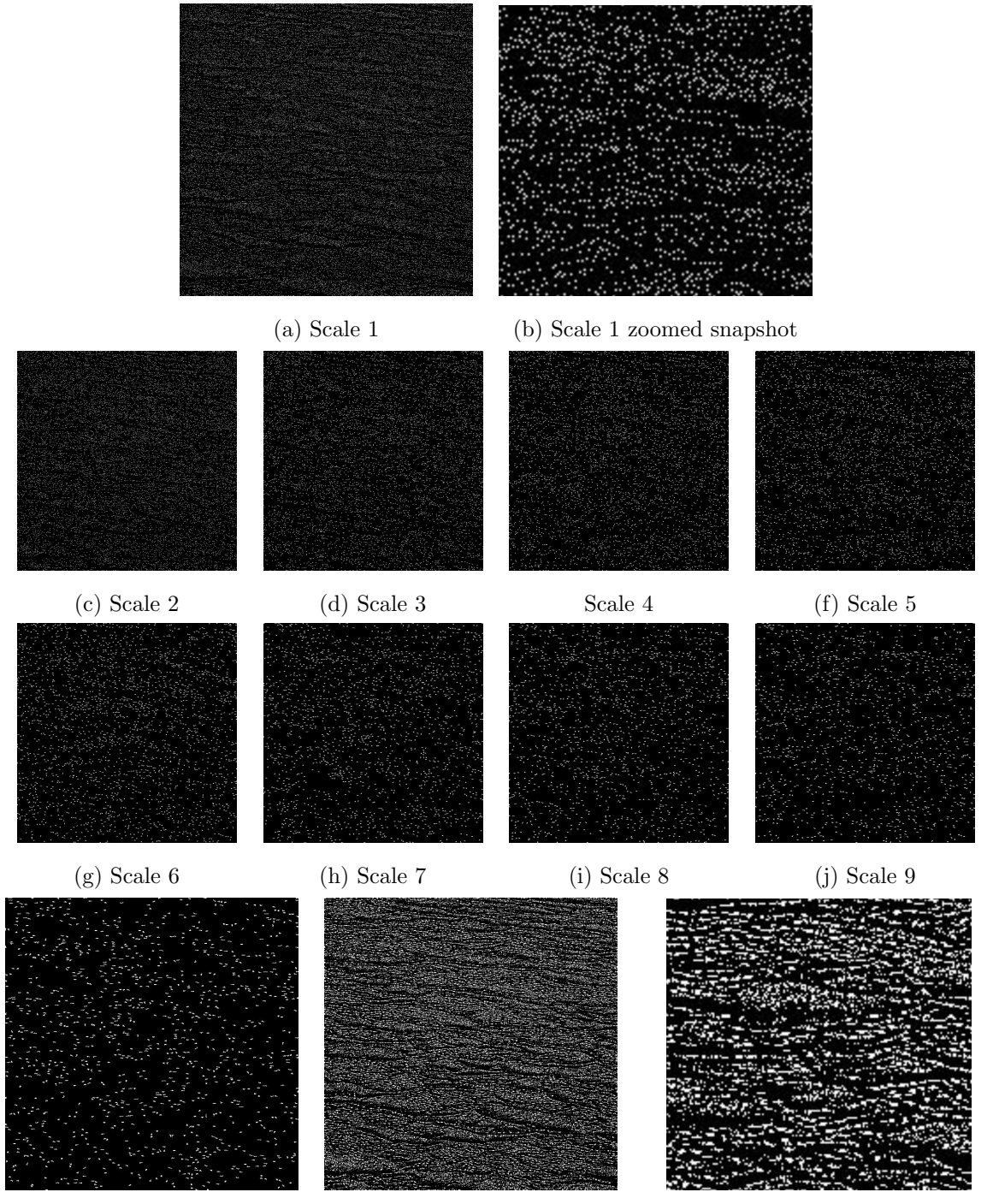

(a) Scale 1 (b) Scale 1 zoomed snapshot

(c) Scale 2 (d) Scale 3 Scale 4 (f) Scale 5

(g) Scale 6 (h) Scale 7 (i) Scale 8 (j) Scale 9

(k) Scale 10 (l) Scales 1 to 10 (m) Scale 1 to 10 zoomed snapshot

Figure 2: Illustration of the pulse patterns at various scales of the DPT for image (a) in Figure 1

The DPT is obtained via iterative application of the operators L_n, U_n with n increasing from 1 to N, decomposing the image into a number of pulses ϕ_{ns} using the operations $P_n = L_n \circ U_n$ or $P_n = U_n \circ L_n$ and $Q_n = P_n \circ P_{n-1} \circ ... \circ P_1$. At each iteration we retain the portions of the image which are filtered out by the application of $P_n(f),\ n = 1, 2, ..., N$ i.e. $(I - P_n)(f) = D_n(f)$, until we obtain $Q_N(f)$, a constant function, where I is the identity operator. The function f is then decomposed as the DPT of f:

$$f = \sum_{n=1}^{N} D_n(f) = \sum_{n=1}^{N} \sum_{s=1}^{\gamma(n)} \phi_{ns}.$$

This image decomposition provides us with information about the content of the image at all scales from $n = 1$ up to N. The number of pulses at scale n, $\gamma(n)$, decreases exponentially as n increases.

To illlustrate the DPT extraction of pulses from an image we apply it to the image in Figure 1(a) and extract the pulses given in Figure 2. Only the small scales, namely 1 to 10, are shown. Note that the largest scale is $640^2 = 409600$. It is clear the DPT thus presents a computationally heavy problem. Advances in this have however been developed through a graph based algorithm [4, 26], which has the added advantage of an accessible structure of the DPT pulses and their values.

The scale 1 pulses in Figure 2(a) replicate the texture of the image. The texture becomes less visible with increasing scale from 2 up to 10. However, combining scale 1 to 10 in Figure 2(l) shows a strong texture extraction. The scale 1 to 10 for the other example images are also shown in Figure 3. The DPT thus provides useful information for the texture of an image in the small scale range. Figure 4 illustrates the pulse numbers $\gamma(n)$ across scales to 1100 for image (a), indicating that pulses in scales 1 to 10 covers approximately 80% of the total number of pulses. The details of the image, namely the texture, are extracted in the small scales and the background shading in the remainder of the pulses sizes. This is similarly observed for image (b) - (d). Note that the scale and pulses contain relevant image information as the image is assumed to be free from noise here.

3. An inhomogeneous cluster model

Consider a point process $Z(x)$ on $\mathbb{Z}^2$, for the case of images. Here the spatial domain is divided into a grid representing the pixels, and $Z(x)$ represents the spatial function with value equal to the pixel luminosity at pixel position x [27, Section 3.6]. For each pixel in a pulse, that is, a white pixel in the images in Figure 3, a point in the point pattern is allocated at the centre of that pixel position on the pixel constructed window. `Spatstat` [27] allows for defining a discrete window and the extracted point pattern can be modeled on this discrete window. This modelling approach was also implemented (but not included in the paper) on a pixel domain instead of a continuous window. The resulting fits are identical and the discrete domain approach adds in more computational need to an already high computational problem. The approach presented in the paper thus sticks to the continuous window.

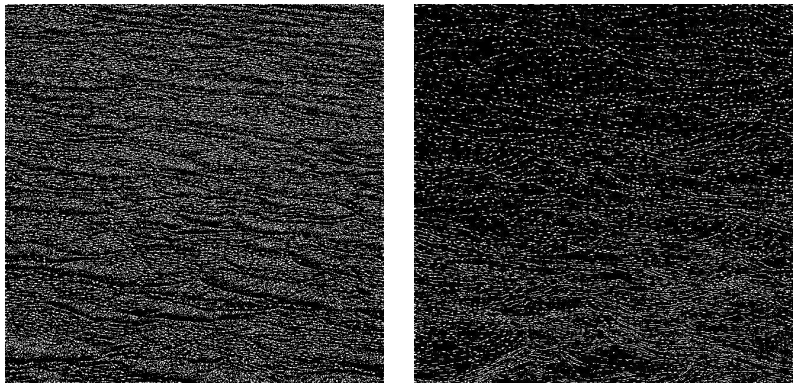

(a) 77091; 0.1882 (b) 42536; 0.1038

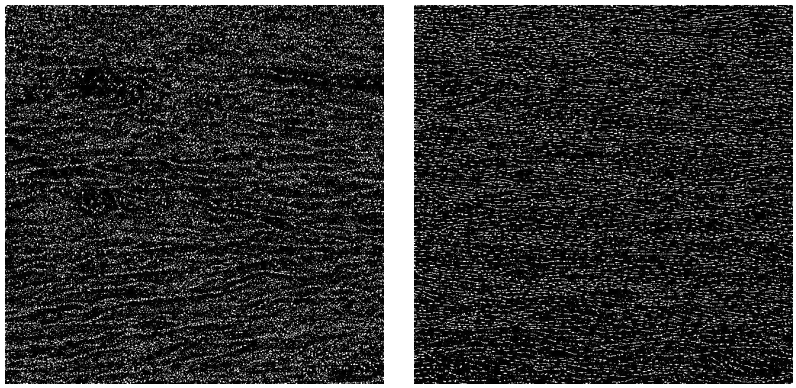

(c) 54200; 0.1323 (d) 49253; 0.1202

Figure 3: DPT pulses for scales 1 to 10 extracted for the images in Figure 1(a) - (d) respectively, with the number of points of the extracted point pattern and the average intensity shown below each

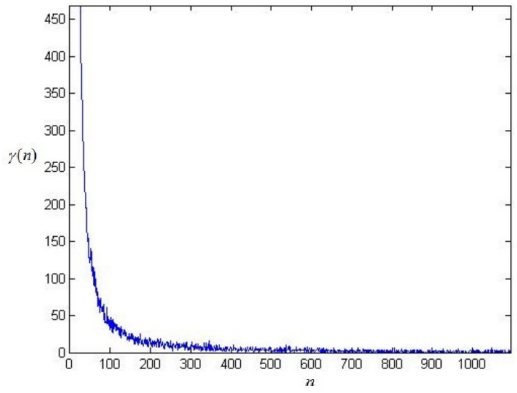

Figure 4: Pulses numbers $\gamma(n)$ at the smaller scales $n = 1, 2, ..., 1100$ for image (a)

The modeling is however done in a continuous manner. This is not counter intuitive as an image is a discrete realisation of a continuous real-world construct. The continuous modeling can thus be justified. Implementation in `spatstat` none-the-less outputs pixellated values post-fitting. Note that for scale 1 in the DPT of any image no pixels are direct neighbours of any other pixels when using 4-connectivity, that is neighbours above, below, left and right $\{(i, j+1), (i, j-1), (i-1, j), (i+1, j)\}$, but for scale 2, and higher scales, the pixels can have direct 4-connected neighbours. The scale 1 extracted point pattern thus exhibits a natural inhibition at distance of two pixel lengths (the minimum distance between two unconnected pixels). We thus model the point patterns extracted from Figure 3 to allow for the incorporation of the pattern visible but without the inhibition present if only scale 1 is used. The inhibition of 1 ixel length is unavoidable though.

Formally a point process $Z(x)$ is stationary if its distribution is invariant under translations, where its distribution refers to, in the simplest terms, the number of points per unit area. Here we investigate modelling for the nonstationarity in a very large clustered process. A cluster is a group of points whose pair distances are less than the pair distances in the whole pattern (measured in some appropriate manner) and eludes to stochastic dependence between points [28]. This difference is at least second order as opposed to the first order property of stationarity and should not be confused.

The clustered structure of the water images' DPT pulses lead us to fit a Matérn cluster process model, a special case of the Neyman-Scott process, to the point patterns extracted from the discrete pulses in Figure 3. A Neyman-Scott spatial cluster point process models parent points as a homogeneous Poisson process with intensity κ with offspring distributed isotropically around the parent points with distances according to a density $f_\tau(r)$ and with number of offspring to each parent a random M with some distribution with mean ν [29]. For the Matérn cluster process [30] the density is determined so that, conditionally on the location of the cluster centres, the realised points x_i are uniformly distributed in the ball $b(c_i, s)$ centered at c_i of radius s, and for $c_i \in C$, where C is the point process of the parent points. For the homogeneous case the cluster centres (parent points) are a Poisson process, at which offspring points are assumed as a second Poisson model in a disc of radius s (homogeneous and with mean ν) around each parent point independently and uniformly. To incorporate inhomogeneity into the offspring we can use the approach of [31] which allows for inhomogeneity of the intensity by applying thinning to the parent points.

The Matérn cluster model is appropriate by representing each pulse as a cluster, that is the offspring points form each wave. In `spatstat` [27] the inhomogeneity can be emulated by estimating an inhomogeneous fitted intensity image function. This is done while using the `kppm` function with the Matérn cluster option. For the point patterns extracted from images (a) to (d) in Figure 3 the trend $\lambda(u) = \exp(\beta_0 + \beta_1 x + \beta_2 y)$ is fitted to capture the inhomogeneity in the vertical and horizontal directions, with parameters β_0, β_1 and β_2, and x and y the image axes.

Parameter		Estimate	SE	2.5% CI	97.5% CI
$\hat{\beta}_0$	Image (a)	-1.78	9.68×10^{-3}	-1.80	-1.76
	Image (b)	-1.97	1.24×10^{-2}	-1.99	-1.94
	Image (c)	-2.08	1.15×10^{-2}	-2.10	-2.06
	Image (d)	-2.25	1.22×10^{-2}	-2.28	-2.23
$\hat{\beta}_1$	Image (a)	5.19×10^{-5}	1.95×10^{-5}	1.36×10^{-5}	9.01×10^{-5}
	Image (b)	0.0004	2.63×10^{-5}	0.0003	0.0004
	Image (c)	9.83×10^{-5}	2.33×10^{-5}	5.27×10^{-5}	0.00014
	Image (d)	-0.0001	2.44×10^{-5}	-0.00015	-0.00005
$\hat{\beta}_2$	Image (a)	2.96×10^{-4}	1.95×10^{-5}	2.57×10^{-4}	3.34×10^{-4}
	Image (b)	-0.0014	2.68×10^{5}	-0.0015	-0.0014
	Image (c)	7.46×10^{-5}	2.33×10^{-5}	2.90×10^{-5}	0.00012
	Image (d)	0.00051	2.45×10^{-5}	0.00046	0.00056

Table 1: Parameter estimates, standard errors and confidence intervals for the intensity fit parameters of the scale 1 to 10 point patterns in Figure 1

Log Gaussian Cox processs (LGCP's) [32] are also cluster processes that could be fitted to the point patterns considered here. The logical nature of the Matérn process through the parent and simple sibling processes fits the structure of wave pulses in the original image, however, being therefore the focus here. Alternative cluster point process models, including the LGCP, were also fitted giving similar fit strengths which is futher discussed next for the Matérn point process model.

4. Results and Discussion

We focus on the point patterns for the scale 1 to 10 pulses of the DPT for each of the sample images In Figure 2, as the pattern represents a large point pattern with useful structural information of the image, as already discussed and shown in Figure 2. The inhomogeneity of these patterns is confirmed by estimating the intensity $\lambda(u) = \exp(\beta_0 + \beta_1 x + \beta_2 y)$ using the `density.ppp` function of the `spatstat` package of `R` and is visible in Figure 5. The bandwidth chosen was selecting using Scott's method [27] and provides an intensity which captures the structure without smoothing too much. The fitted trend parameters are shown in Table 1 for the scale 1 to 10 extracted point patterns of the sample images. The confidence intervals and standard errors for these fitted parameters are also provided in Table 1. The standard errors and confidence intervals indicate the strength of the inhomgeneity fitted.

Using the `Jinhom` function of the same package [33] the clustered nature of the point pattern is

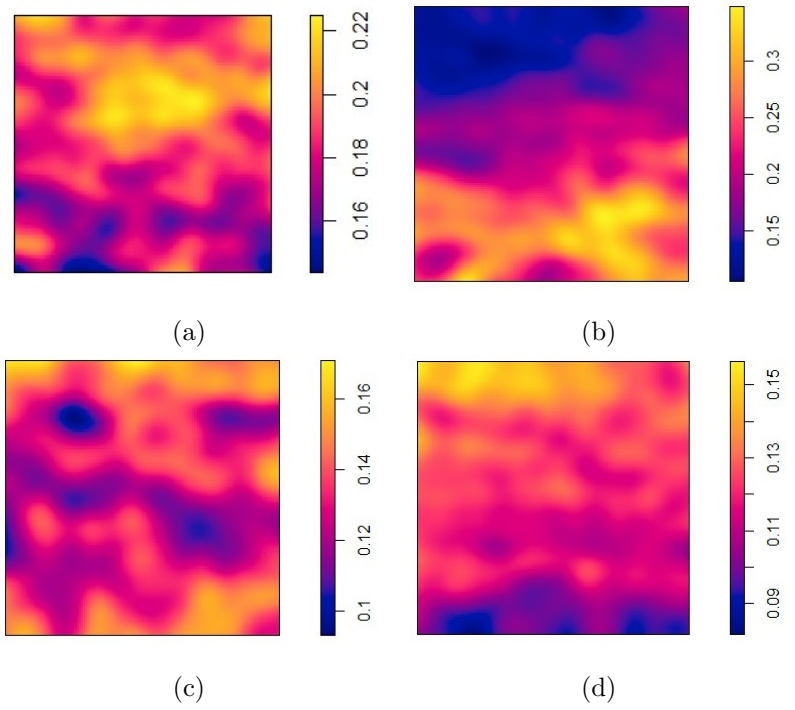

Figure 5: The kernel-fitted intensity for the point patterns of the scale 1 to 10 pulses plotted in two dimensions using bandwidth selected by Scott's method

confirmed as the fitted functions are below 1. Figure 6 shows these graphs. The stepped nature in the fit is due to the pixellated data. Note that the inhomogeneous K-function cannot be applied to this data as it is only implementable for point patterns of up to size 1000. It is a computationally heavy calculation with solutions recently propsed in [34] and [35] using parallel programming with cloud computing and GPUs.

The fitted inhomogeneous J-Function shows clustering for $r \geq 1$ since the points represent pixels thereby introducing an automatic inhibition for $r < 1$. Note that r effectively refers to the pixels, that is, $r = 1$ implies one pixel length. The DPT acts at a pixel level so even at a different pixel resolution r will always be interpretable as the pixel lengths. All images in Figure 1 (a) -(d) considered here have similar resolution and are thus comparable. As r increases the clustering gains strength. The inhibition for $r < 1$ is visibly picked up as a regular pattern here as well, except for image (b) which is the smallest pattern of the four.

Using the `kppm` function of `spatstat` the fitted Matérn model has a fitted parameters $\hat{\kappa}$ (the parent parameter) and $\hat{s}$ (the radius of the offspring process). The fitted parameters for the four images are shown in Table 2. There is a distinct difference in the simulations versus the real images.

In Figure 7 the residuals of these fitted models are plotted. It is clear that there is still pattern left in the residuals which is undesirable. Figure 8 shows these residuals as a histogram. Diagnostics

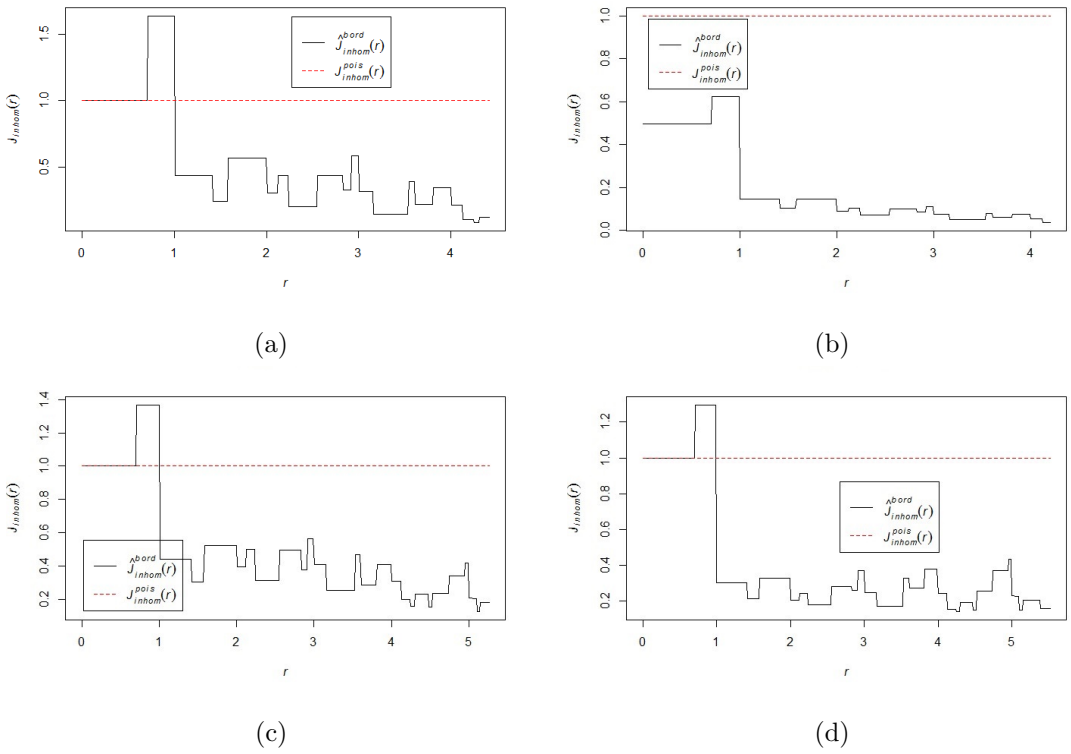

Figure 6: Fitted inhomogeneous J-functions on the points patterns extracted from the images (a) - (d) respectively

were investigated for the `kppm` modelling, however due to the large size of these point patterns many are not implementable e.g. envelopes. Thus the approach of investigating the residuals is proposed as they are computationally faster (but still not very fast). Thus it is seen that the residuals cluster around two values for all four images.

Since the residuals exhibit pattern a second round of fitting the Matérn cluster process using `kppm` was implemented. The resulting residuals and their histograms of the second fit are shown in Figures 9 and 10 respectively.

It is now visible that the pattern has been removed and a good fit attained. This modeling approach is hierarchical in nature and provides a new approach to modeling the pulses of the DPT for these sample images. All the alternative fits of the cluster models using `kppm` showed similar patterned residuals to those in Figure 7, but with heavier computational requirements. The Matérn cluster model provides a simple approach and showcases the hierarchical fitting presented here.

The residuals were also tested for CSR usig the J-function, see Figure 11. No clustering is present, and a regular nature present for all four images.

	$\hat{\kappa}$	$\hat{s}$
Image (a)	45.17	10.38
Image (b)	0.11	2.22
Image (c)	0.098	4.87
Image (d)	0.196	1.77

Table 2: Fitted Matérn cluster point process parameters for images (a) - (d)

5. Discussion

Here we present a unique fitting of the Matérn model to an inhomogeneous point pattern of a large size extracted from image constructs, namely the pulses obtained using the DPT. The pulses from the DPT naturally model the patterns present in an image, as seen in Figure 1. The merging of this type of spatial modelling to pattern analysis in images is novel and the results show that the merger has been powerful and is applicable to similar types of images.

Further investigation into spatial modelling for such image constructs, however, warrants attention. It is known in image analysis that pixels nearby exhibit dependence structures. This is most commonly simplified to 4-connectivity. However, spatial statistics allows for more sophisticated correlation structures. This start of such modeling is shown in this paper. In addition a hierarchical cluster model is fitted which has not been investigated to our knowledge and shows a promising approach to complex large point patterns. The simulation of such a process could be theoretically advanced using a recently proposed approach such as that of Mastrantonio, Gelfand and Lasinio in [36].

Further work on an appropriate covariance structure could also build towards enabling a full reconstruction of the original image using the fitted hierarchical model. The inhomogeneous nature has been captured through the fitted intensity however the parameter κ and s are isotropic in their nature leading to a non-perfect reconstruction at the first level of fitting - the inter-pixel correlation is not yet captured. Stochasticity of κ and s could also assist in capturing the complexity of these point patterns extracted using the DPT. The computational issues in these approaches would have to be carefully considered however.

In addition, here we focus on a greyscale (one-dimensional) image. The modelling of RGB, HSV or multispectral images presents an interesting spatial data set with possible important extensions of the current methodology. Their large sizes will present a challenge, in particular in standard software packages like `spatstat`, and will require a further very careful programming. In this sense, the methods could become further of interest in the big data domain, following the work in [34, 35]. In addition, time could be an additional consideration when looking at videos i.e. sequences of videos. The spatio-temporal modeling may present mechanisms for image analysis tasks such as object tracking.

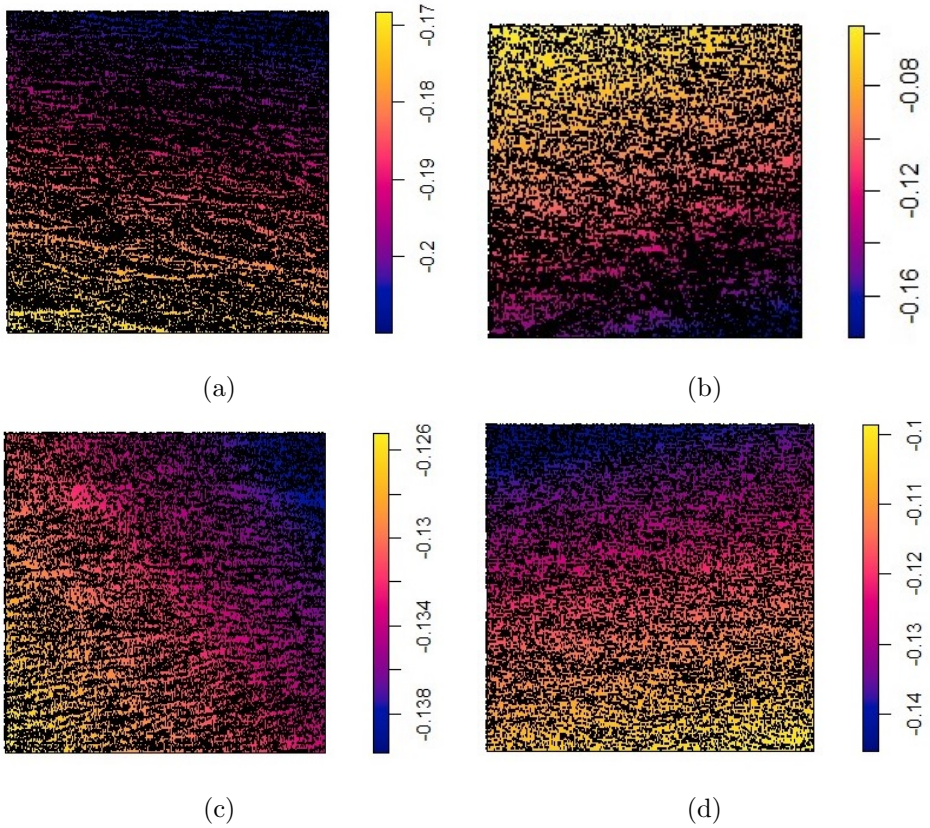

Figure 7: Plots of the residuals of the fitted Matérn point processes to images (a) - (d)

Signal analysis currently receives much attention in the literature due to growth in the fields of artificial intelligence and machine learning. The merger of spatial statistics and image analysis allows for a wider scope of approaches, and most importantly the incorporation of stochasticity in a domain governed by uncertainty of observations and spatial dependence. Recognition and quantification of point patterns, possibly extended towards linear features and other types of objects may lead to a better understanding of the process in nature or in image processing that is represented by individual images. In addition, a further development of the current methods may result in the reconstruction of images from separate, smaller, datasets and hence to a storage of images that is both easily accessible and transferable.

6. Conclusion

This paper presented a novel application of a spatial cluster point process, the Matérn cluster model, to model constructs extracted from images using the Discrete Pulse Transform. The pulses of scales $n = 1, 2, 3, ..., 10$ from the DPT were modelled as a hierarchical point pattern and the fit

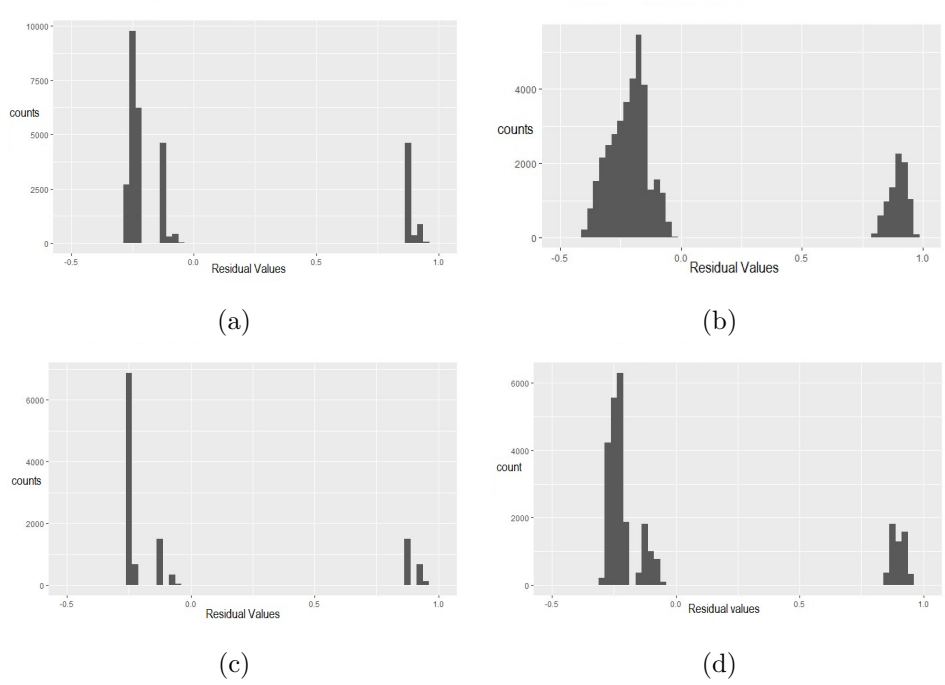

Figure 8: Histograms of the residuals shown in Figure 7

achieved shown to be good.

Alternatively the shape of pulses could be considered and the extracted pattern then modeled as a marked point process. More of the structure could be extracted in this manner. In addition, other image types, e.g. RGB, can be incorporated making the problem a multidimensional point pattern. Both these approaches will need careful computational consideration.

The point pattern modeled herein is large leading this type of modelling into the big data domain as the scale n is increased and incorported into the pattern. Already, many functions of `spatstat` cannot handle the size of the point pattern, for example the inhomogeneous K-function and pair correlation function.

Further investigation into simulating the original image from this hierarchical fit should be investigated. In addition to capture more of the interaction between points a Cox process could be fitted [37]. This allows for randomness in the intensity coefficients and could enable modelling and more precise resimulation of the point patten. A modified Thomas process with Gaussian clusters with anisotropic variance is also a possibility. Here we present an initial investigation into the strength of modelling the pulses of the DPT spatially.

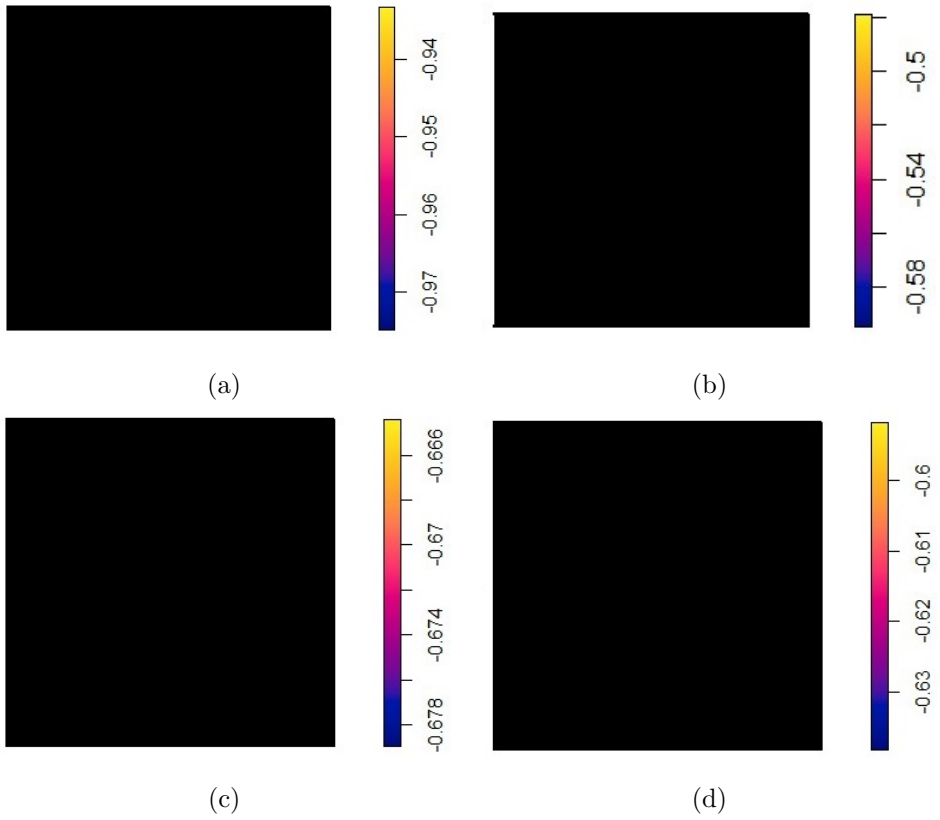

Figure 9: Plots of the residuals of the fitted Matérn point processes to the residuals of images (a) - (d)

Acknowledgements

This work is based on the research supported in part by the National Research Foundation of South Africa (SARChI Research Chair- UID: 71199). Opinions expressed and conclusions arrived at are those of the authors and are not necessarily to be attributed to the NRF.

References

[1] R. Anguelov, I. Fabris-Rotelli, LULU operators and discrete pulse transform for multidimensional arrays, Image Processing, IEEE Transactions on 19 (11) (2010) 3012–3023.

[2] I. Fabris-Rotelli, K. van Oldenmark, P. J. van Staden, Evaluation of noise removal in signals by LULU operators, in: Proceedings of the 2010 SASA Conference, Potchefstroom University, 8 12 November 2010,.

[3] I. Fabris-Rotelli, The Discrete Pulse Transform for images with entropy-based feature detection,

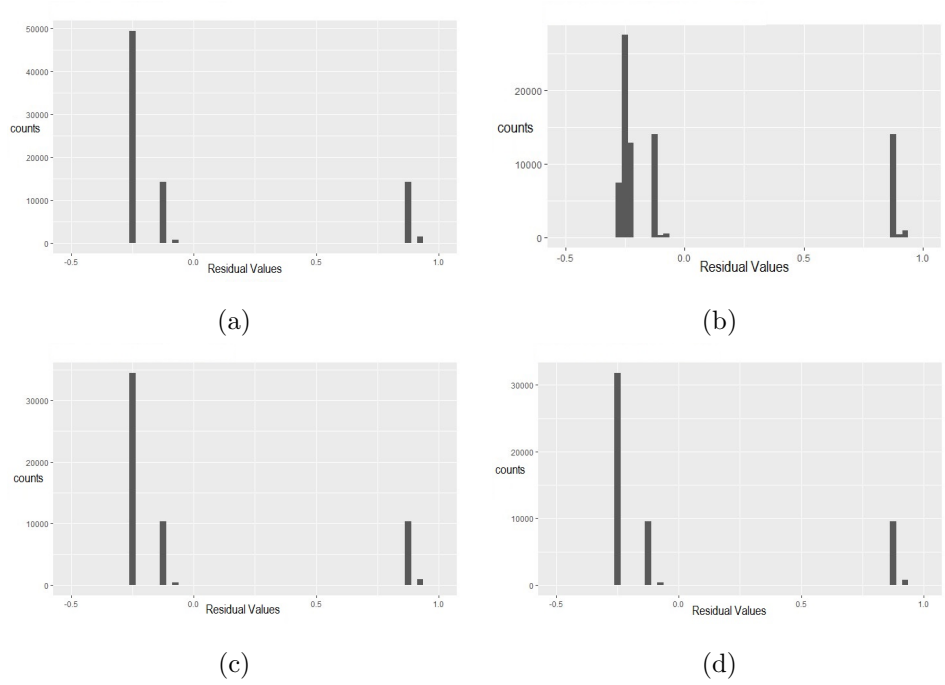

Figure 10: Histograms of the residuals of the fitted residual model shown in Figure 9

in: P. Robinson, A. Nel (Eds.), Proceedings of the 22nd Annual Symposium of the Pattern Recognition Association of South Africa, 22 -25 November 2011, pp. 43 – 48.

[4] G. Stoltz, I. Fabris-Rotelli, Pulse reformation algorithm for leakage of connected operators, in: Proceedings of the International Conference on Computer Vision Theory and Applications (VISAPP 2015), Berlin, Germany, 11-14 March 2015, pp. 583–590.

[5] R. Rahmat, A. S. Malik, N. Kamel, H. Nisar, 3D shape from focus using LULU operators and Discrete Pulse Transform in the presence of noise, Journal of Visual Communication and Image Representation 24 (3) (2013) 303–317.

[6] D. S. Velidou, V. Tolpekin, A. Stein, T. Woldai., Use of Gestalt theory and random sets for automatic detection of linear geological features, Mathematical Geosciences 47 (3) (2015) 249–276.

[7] R. S. Fraser, S. Mattoo, E.-N. Yeh, C. McClain, Algorithm for atmospheric and glint corrections of satellite measurements of ocean pigment, Journal of Geophysical Research: Atmospheres (1984–2012) 102 (D14) (1997) 17107–17118.

[8] B.-C. Gao, M. J. Montes, R.-R. Li, H. M. Dierssen, C. O. Davis, An atmospheric correction algorithm for remote sensing of bright coastal waters using modis land and ocean channels in

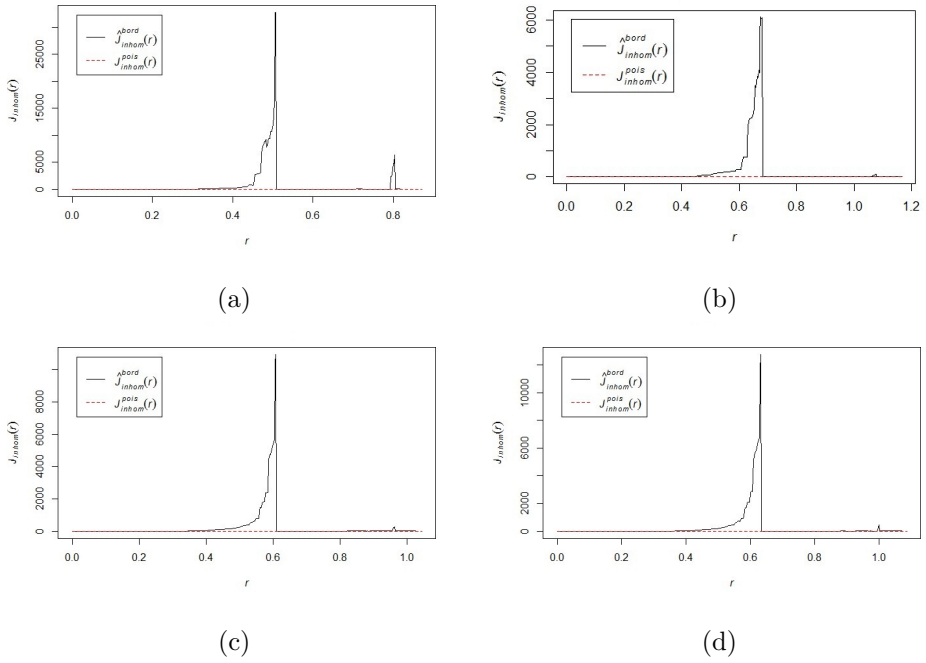

Figure 11: Fitted inhomogeneous J-function to the residuals of the second fit of the Matérn cluster process

the solar spectral region, Geoscience and Remote Sensing, IEEE Transactions on 45 (6) (2007) 1835–1843.

[9] M. D. Mermelstein, E. Shettle, E. Takken, R. Priest, Infrared radiance and solar glint at the ocean-sky horizon, Applied Optics 33 (25) (1994) 6022–6034.

[10] J. Beard, Reduction of solar glints from the sea with a linear polarizer, Tech. rep., Infrared and Optics Devision, Naval Weapons Centre, China Lake, CA (1976).

[11] F. Bréon, N. Henriot, Spaceborne observations of ocean glint reflectance and modeling of wave slope distributions, Journal of Geophysical Research: Oceans (1978–2012) 111 (C6) (2006) 1–10.

[12] S. Kay, J. D. Hedley, S. Lavender, Sun glint correction of high and low spatial resolution images of aquatic scenes: a review of methods for visible and near-infrared wavelengths, Remote Sensing 1 (4) (2009) 697–730.

[13] R. Doerffer, H. Schiller, J. Fischer, R. Preusker, M. Bouvet, The impact of sun glint on the retrieval of water parameters and possibilities for the correction of meris scenes, in: Proceedings of the 2nd MERIS/(A) ATSR User Workshop, ESA SP-666,(ESA, Frascati, Italy, 2008), 2008.

[14] A. Fournier, W. T. Reeves, A simple model of ocean waves, in: ACM Siggraph Computer Graphics, Vol. 20, 1986, pp. 75–84.

[15] Y. Zhao, M. Zhang, H. Chen, An efficient ocean sar raw signal simulation by employing fast fourier transform, Journal of Electromagnetic Waves and Applications 24 (16) (2010) 2273–2284.

[16] D. Hinsinger, F. Neyret, M.-P. Cani, Interactive animation of ocean waves, in: Proceedings of the 2002 ACM SIGGRAPH/Eurographics symposium on Computer animation, 2002, pp. 161–166.

[17] W. R. Alpers, C. Bruening, On the relative importance of motion-related contributions to the sar imaging mechanism of ocean surface waves, Geoscience and Remote Sensing, IEEE Transactions on GE-24 (6) (1986) 873–885.

[18] J. Tessendorf, Simulating ocean water, Simulating Nature: Realistic and Interactive Techniques. SIGGRAPH 1 (2001) 1–26.

[19] P. Penven, P. Marchesiello, L. Debreu, J. Lefèvre, Software tools for pre-and post-processing of oceanic regional simulations, Environmental Modelling & Software 23 (5) (2008) 660–662.

[20] A. F. Shchepetkin, J. C. McWilliams, The regional oceanic modeling system (roms): a split-explicit, free-surface, topography-following-coordinate oceanic model, Ocean Modelling 9 (4) (2005) 347–404.

[21] J. T. Haleson, Understanding natural texture, Tech. rep., University of Rochestor (1977).

[22] F. M. Vilnrotter, R. Nevatia, K. E. Price, Structural analysis of natural textures, Pattern Analysis and Machine Intelligence, IEEE Transactions on PAMI-8 (1) (1986) 76–89.

[23] Y. Liu, W.-C. Lin, J. Hays, Near-regular texture analysis and manipulation, in: ACM Transactions on Graphics (TOG), Vol. 23, 2004, pp. 368–376.

[24] J. Serra, Image Analysis and Mathematical Morphology, Volume II: Theoretical Advances, chapter Mathematical Morphology for Boolean Lattices, Academic Press, London, 1988.

[25] V. L., Shape in Picture. NATO ASI Series (Series F: Computer and Systems Sciences),, Vol. 126, Springer, Berlin, Heidelberg, 1994, Ch. Morphological Area Openings and Closings for Grey-scale Images.

[26] D. P. Laurie, The roadmaker's algorithm for the Discrete Pulse Transform, IEEE Transactions on Image Processing 20 (2) (2011) 361–371.

[27] A. Baddeley, E. Rubak, R. Turner, Spatial point patterns: Methodology Applications with R, CRC Press, 2016.

[28] P. Diggle, Statistical Methods for Spatio-temporal Systems, Chapman & Hall/CRC, 2007, Ch. Spatio-temporal point processes: methods and applications, pp. 1–45.

[29] U. Tanaka, Y. Ogata, D. Stoyan, Parameter estimation and model selection for Neyman-Scott point processes, Biometrical Journal: Journal of Mathematical Methods in Biosciences 50 (1) (2008) 43–57.

[30] B. Matérn, Lecture Notes in Statistics, Springer-Verlag, New York, 1986, Ch. Spatial Variation.

[31] R. Waagepetersen, An estimating function approach to inference for inhomogeneous Neymen-Scott processes, Biometrics 63 (2007) 252–258.

[32] J. Moller, A. Syversveen, R. Waagepetersen, Log Gaussian Cox processes, Scandinavian Journal of Statistics 25 (1998) 451482.

[33] M. van Lieshout, A J-function for inhomogeneous point processes, Statistica Neerlandica 65 (2) (2011) 183–201.

[34] G. Zhang, Q. Huang, A.-X. Zhu, J. Keel, Enabling point pattern analysis on spatial big data using cloud computing: optimizing and accelerating Ripley's k function, International Journal of Geographical Information Science 30 (11) (2016) 2230–2252.

[35] W. Tang, W. Feng, M. Jia, Massively parallel spatial point pattern analysis: Ripley's k function accelerated using graphics proprocess units, International Journal of Geographical Information Science 29 (3) (2015) 412–439.

[36] G. Mastrantonio, A. E. Gelfand, G. J. Lasinio, The wrapped skew Gaussian process for analyzing spatio-temporal data, Stochastic environmental research and risk assessment 30 (8) (2016) 2231–2242.

[37] D. Cox, Some statistical models related with series of events, Journal of the Royal Statistical Society, Series B 17.